Development 138, 1935-1945 (2011) doi:10.1242/dev.056861

Neuron navigator 3a regulates liver organogenesis during zebrafish embryogenesis

Christian Klein[1], Janine Mikutta[1], Janna Krueger[1,2], Katja Scholz[1], Joep Brinkmann[1], Dong Liu[1], Justus Veerkamp[3], Doreen Siegel[4], Salim Abdelilah-Seyfried[3] and Ferdinand le Noble[1,2,*]

SUMMARY

Endodermal organogenesis requires a precise orchestration of cell fate specification and cell movements, collectively coordinating organ size and shape. In *Caenorhabditis elegans*, *uncoordinated-53* (*unc-53*) encodes a neural guidance molecule that directs axonal growth. One of the vertebrate homologs of *unc-53* is neuron navigator 3 (*Nav3*). Here, we identified a novel vertebrate neuron navigator 3 isoform in zebrafish, *nav3a*, and we provide genetic evidence in loss- and gain-of-function experiments showing its functional role in endodermal organogenesis during zebrafish embryogenesis. In zebrafish embryos, *nav3a* expression was initiated at 22 hpf in the gut endoderm and at 40 hpf expanded to the newly formed liver bud. Endodermal *nav3a* expression was controlled by Wnt2bb signaling and was independent of FGF and BMP signaling. Morpholino-mediated knockdown of *nav3a* resulted in a significantly reduced liver size, and impaired development of pancreas and swim bladder. In vivo time-lapse imaging of liver development in *nav3a* morphants revealed a failure of hepatoblast movement out from the gut endoderm during the liver budding stage, with hepatoblasts being retained in the intestinal endoderm. In hepatocytes in vitro, *nav3a* acts as a positive modulator of actin assembly in lamellipodia and filipodia extensions, allowing cellular movement. Knockdown of *nav3a* in vitro impeded hepatocyte movement. Endodermal-specific overexpression of *nav3a* in vivo resulted in additional ectopic endodermal budding beyond the normal liver and pancreatic budding sites. We conclude that *nav3a* is required for directing endodermal organogenesis involving coordination of endodermal cell behavior.

KEY WORDS: Neuron navigator 3a, Liver development, Neural guidance genes, Intestinal endoderm, Zebrafish

INTRODUCTION

Liver organogenesis requires an intricate genetic network that spatiotemporally controls hepatoblast specification and migration. Movement of hepatocyte precursors out from the gut endoderm is a key event during initiation of liver organogenesis (Bort et al., 2006; Margagliotti et al., 2007; Sosa-Pineda et al., 2000). Within a close time frame in zebrafish embryogenesis, adjacent endodermal cell populations, such as hepatic and pancreatic precursors, migrate to their determined destination. Liver specification is mediated by Wnt2bb expression in the lateral plate mesoderm, fibroblast growth factors (FGFs) derived from the cardiac mesoderm and bone morphogenetic proteins (BMPs) secreted by the septum transversum mesenchyme (Calmont et al., 2006; Goessling et al., 2008; Jung et al., 1999; Ober et al., 2006; Rossi et al., 2001; Si-Tayeb et al., 2010). Although the molecular regulation of endodermal specification events is starting to be unraveled, surprising little is known about the control of endodermal cell movements in the context of shaping organs such as liver and pancreas.

Coordinated guidance of cells occurs during the early phases of liver ontogenesis. During liver budding in zebrafish, cells of the nascent liver form a mass of hepatoblasts that migrates out of the foregut endoderm as a compact structure. In mammals, hepatocytes dissociate from one another and migrate into the mesenchyme of the adjacent septum transversum by 'interstitial invasion' (Elias, 1955). It is still unclear how 'interstitial invasion' or hepatoblast movements are initiated and directed, and which intracellular processes actually control the physical movement of liver cells or compacted hepatoblasts. In general, extensive remodeling of actin filaments at the cell surface of migrating cells is needed for cellular movement. Lamellipodia and filipodia are characteristic features at the leading edge of motile cells. Lamellipodia contain cross-linked networks of actin filaments, and filipodia contain tensile structures composed of bundled F-actin that probe the extracellular environment for guidance cues (Huber et al., 2003; Tran et al., 2007). Whereas lamellipodia are generally considered to be the motor of forward movement during cell migration, filipodia are essential for the direction of motion.

Neural guidance genes play a central role in shaping the developing nervous system by mediating neuronal cell migration and neural connectivity. In the axonal growth cones of developing nerves, neural guidance molecules control movement by conveying attractive or repulsive guidance cues into actin remodeling events in lamellipodia and filipodia extensions (Huber et al., 2003). Recent evidence suggests that this unique function of neural guidance genes also extends to the developing vascular system. It has recently been shown that the neural guidance protein encoded by *Unc5b*, a mammalian homolog of *Caenorhabditis elegans uncoordinated-5* (*unc-5*), also controls endothelial tip cell behavior of expanding angiogenic sprouts, thereby controlling morphogenesis of the developing vasculature (Lu et al., 2004). The concept that emerged from this study is that during evolution, neural guidance gene function has been co-opted by the developing vascular system to control morphogenesis. Here, we investigated whether neural

[1]Department of Angiogenesis and Cardiovascular Pathology, Max-Delbrueck-Center for Molecular Medicine (MDC), D-13125 Berlin, Germany. [2]Center for Stroke Research Berlin (CSB), 10117 Berlin, Germany. [3]Department of Epithelial Polarity and Zebrafish Genetics, Max-Delbrueck-Center for Molecular Medicine (MDC), D-13125 Berlin, Germany. [4]Institute of Biochemistry, University of Ulm, D-89091, Ulm, Germany.

*Author for correspondence (lenoble@mdc-berlin.de)

Accepted 16 February 2011

guidance genes might also be involved in controlling endodermal organogenesis. We focused on neuron navigator 3 (*Nav3*), the vertebrate homolog of the *C. elegans* gene *uncoordinated-53* (*unc-53*), and discovered a novel functional role in endodermal cell movements, regulating liver morphogenesis in zebrafish.

Unc-53 in *C. elegans* encodes a neural guidance factor required for axon elongation and cell migration (Maes et al., 2002; Schmidt et al., 2009; Stringham et al., 2002). In mammals, three *unc-53* homolog genes exist: neuron navigator 1, 2 and 3 (*Nav1*, *Nav2* and *Nav3*) (Maes et al., 2002). Both the *unc-53* gene in *C. elegans* and *Nav3* in rat and human have different isoforms (Maes et al., 2002; Peeters et al., 2004; Schmidt et al., 2009). Intracellular protein localization, tissue specific expression and differential relevance of UNC-53 or Nav3 protein isoforms have not been clarified so far. Data from *C. elegans* suggest that, in particular, the longest isoform *unc-53L* is essential for neuronal cell migration involving a specific interaction with components of the actin assembling complex, thus providing a linkage between extracellular guidance cues and intracellular cytoskeleton remodeling (Schmidt et al., 2009; Stringham et al., 2002). Here, we identified two previously uncharacterized *nav3* homologs in zebrafish. The longer isoform *nav3a* is highly homologous to *unc-53L* and is expressed in the intestinal endoderm in structures that give rise to the liver.

In vivo knockdown of *nav3a* in zebrafish impaired the movement of hepatoblasts out from the gut endoderm, resulting in a significantly reduced liver size. In vitro, *nav3a* was found to be linked to the actin-assembling protein complexes in lamellopodia and filipodia extensions of moving cells, and to have a strong impact on actin polymerization dynamics controlling hepatocyte movement. Overexpression of *nav3a* resulted in aberrant movement of endodermal cells, and formation of ectopic endodermal buds. Our study identified a unique and previously unknown role for *neuron navigator-3a* in endodermal cell movement controlling liver size, and furthermore highlights the important contribution of neural guidance genes in tissue morphogenesis.

MATERIALS AND METHODS

Isolation and cloning of *nav3a*

We identified the 3′ and 5′ ends of the *nav3* isoform by RACE PCR using the Clontech RACE-Kits on first strand cDNA prepared from RNA of zebrafish embryos [22 hours post-fertilization (hpf)]. Northern-Blot of *nav3* isoforms was performed as described previously (Klein et al., 2005) using a probe spanning bp 2350-4347 of *nav3a*.

Cloning of *nav3a* fusion construct and analysis of Nav3a protein localization in vivo and in vitro

We utilized the Gateway Cloning system to generate pDest-Tol2-*sox17-nav3a*-mCherry and pDest-Tol2-*CMV-nav3a*-eGFP plasmids. A 5 kb *sox17* promoter fragment (Reim et al., 2004) was cloned in a Gateway p5′-vector (provided by Didier Stainier, University of California, San Francisco, CA, USA). We cloned a *nav3a* coding region with a mutated *nav3a*-ATG-morpholino binding site (*nav3a*^{ATGmut}) in a Gateway p221-Entry vector (*nav3a*^{ATGmut}*-p221*) and performed the second Gateway reaction in the pDest-Tol2 vector together with a p3′-mCherry construct. As a result we obtained the pDest-Tol2-*sox17-nav3a*^{ATGmut}-mCherry vector. A p5′-CMV-vector (included in the Gateway KIT), Nav3a^{ATGmut}-p221 and p3′-eGFP were used to perform the second Gateway reaction. As a result we obtained the pDest-*CMV-nav3a*^{ATGmut}-eGFP vector.

Injection of morpholino antisense RNA and quantification of emerging liver phenotypes in zebrafish

Embryos of indicated zebrafish strains were injected at the single-cell stage with: 10 ng/embryo *nav3a* ATG morpholino (5′-TTGAAGCAACAC-CAACTACCGGCAT-3′), 10 ng/embryo *nav3a* splice block morpholino (5′-CATCATCAGTCTTACTGACCTTGCA-3′) or 5 ng/embryo *wnt2bb* morpholino (5′-GTGTGCCATATAAAAGTATTCCCCG-3′). Liver phenotypes in *Tg(sox17:GFP)*^{s870} embryos were quantified at the indicated time points using high magnification stereomicroscopy of individual embryos (n=150 embryos per group). Aberrant liver bud (48 hpf) and liver development (120 hpf) was defined as >50% smaller than the mean size of controls. Each experiment was repeated three times. Whole mount DAPI staining was performed in *nav3a*-and control-morpholino-injected *Tg(Sox17:GFP)*^{s870} embryos, and nuclei in the liver bud were counted by confocal imaging.

nav3a^{ATGmut} rescue and gain-of-function experiments

For *nav3a* rescue experiments of *nav3a* morphants and *wnt2bb* morphants, we injected 50 pg of pDest-Tol2-*sox17-nav3a-mCherry* plasmid together with 25 pg Tol2 transposase, and either 10 ng *nav3a*-ATG morpholino or 5ng *wnt2bb* morpholino in single-cell-stage *Tg(sox17:GFP)*^{s870} embryos and analyzed the *nav3a-mCherry* expression and liver bud formation at the indicated time points by confocal microscopy and statistical analysis. For gain-of-function experiments we injected 100 pg of pDest-Tol2-*sox17-nav3a*^{ATGmut}*-mCherry* plasmid together with 25 pg Tol2 transposase in one-cell-stage *Tg(sox17:GFP)*^{s870} embryos and analyzed ectopic budding at the indicated time points.

Zebrafish strains

Zebrafish embryos and adult fish were raised and maintained under standard conditions (Westerfield, 2000). We used the following transgenic lines: *Tg(sox17:GFP)*^{s870} (provided by D. Stainier); Gut-GFP: *Tg(XlEef1a1:GFP)*^{s854} [from the Zebrafish International Resource Center (ZIRC), OR, USA], *Tg(hsp70l:dnBmpr-GFP)* (ZIRC), dnFGF-R-egfp: *Tg*(*hsp70l:dnfgfr1-EGFP*) (ZIRC). Embryos were heat shocked at the 18-somite stage by transferring them into tubes containing pre-warmed egg water on a heat block. *Tg*(*hsp70l:dnBmpr-GFP*) embryos were heat shocked for 30 minutes at 37°C; *Tg*(*hsp70l:dnfgfr1-EGFP*) embryos for 20 minutes at 37°C. At respective time points hemizygous embryos expressing GFP and GFP-negative internal controls were collected and assayed by in situ hybridization.

In situ hybridization

Zebrafish whole mount in situ hybridization (ISH) experiments were performed using the following probes: *nav3a* (amplified with: Fw: 5′-CCACGATAGGAGGACAAA-3′, rv: 5′-GTAGCGGGACAGGATGAA-GAACAG-3); *hhex* (amplified with: Fw: 5′-AGCACCCGCACGGC-CTCTGTA-3′, rv: 5′-GGGTGAACTGATGCTGGTCCTG-3′); *foxa1* (amplified with: Fw: 5′-TATCCAGCAGGCACCCAGCAAAAT-3′, rv: 5′-CTCTAAAGCCGCCGAAGGGTCCAT-3′); *ceruloplasmin* (*cp*, kindly provided by Didier Stainier).

Western blot

Western Blot was performed as described previously (Klein et al., 2003). Detection of Nav3a protein was performed using a zebrafish Nav3a antibody produced by Eurogentec (Belgium) utilizing the AS-SUPR-DXP program. Quantification of Western Blot Nav3 signal was performed using ImageJ software. Signals were normalized with the protein loading visualized with Coomassie stain or tubulin expression (Sigma-Aldrich, T6793).

Confocal time-lapse in vivo imaging of liver budding stages

Single-cell stage *Tg(sox17:GFP)*^{s870} embryos were injected with 10 ng *nav3a* morpholino or 10 ng of control morpholino, anaesthetized at 24 hpf with egg water/tricaine/PTU (0.16 mg/ml tricaine; 1% PTU) and embedded in agarose. Confocal stack pictures of the gut endoderm region were taken at a time interval of 30 minutes over a time period of 30 hours (Zeiss-NLO microscope, 25× objective, Zeiss-ZEN software).

Real-time PCR

Real-time PCR was performed as described previously (Klein et al., 2005). The primers used are listed in Table 1.

Immunofluorescence staining

The following primary antibodies were used: Anti-Nav3a (EUROGENTEC, Belgium; 1:200). Anti-Prox-1 (R+D systems, AF2727; 1:200); Anti-gm130 (B+D Biosystems, 610823; 1:200); anti-Abi-1 (Abcam, 11222; 1:100); monoclonal mouse anti-islet1 (Developmental Studies Hybridoma Bank, clone 39.4D5; 1:100); anti-GFP (Abcam, AB5450; 1:200). Actin filaments were stained with Phalloidin-Alexa Fluor 546 or Phalloidin-Alexa Fluor 633 (Invitrogen, A22283). Nuclei were stained using 6-Diamidino-2-phenylindol (DAPI; Carl Roth, Germany, 6335.1).

Quantification of cell migration in vitro: Scratch assay

We generated *nav3a*-depleted Pac-2 cells by establishing stable anti-*nav3a* shRNA expression. Pac-2 cells were either transfected with anti-Nav3 (GTAAGAACCACAACAATAA) or anti-luciferase (CATCACG-TACGCGGAATACT) cloned short hairpin fragments into shVektor pSUPER (Oligoengine) using the Amaxa Nucleofector Kit according to the manufacturer's instructions. After 3 weeks G418 selection, stable clones were analyzed. *NAV3* depletion in HUH-7 cells was performed by siRNA approach, transfecting siRNA against human *NAV3* (ON-TARGETplus SMARTpool L-018348: GGACUUAACCUAUAUACUA; GAGAGGGUCUUCAGAUGUA; CAGGGAGCCUCUAAUUUAA; GCUGUUAGCUCAGAUAUUU, Dharmacon). Time-lapse imaging was performed with stable Pac-2 cells stably expressing control-shRNA or *nav3a*-shRNA. ImageJ software was used for generating movies. For quantification of the migratory capacity, we performed two parallel scratches in a confluent cell layer, documented three areas per scratch and measured the scratched area at the indicated time points. Migrated area was calculated using ImageJ and Excel software.

Quantification of actin polymerization: FRAP assay

Pac-2 cells stably expressing shRNA against *nav3a* or shRNA against luciferase (control) were transfected with lifeact-RFP (Era et al., 2009; Vidali et al., 2009) plasmid and grown to confluency. Five hours after scratching the Pac-2 monolayer, actin-positive areas of lamellipodia extensions were photobleached by irradiation with a 561 nm laser and subsequently the bleached regions of interest (ROIs) were analyzed by confocal microscopy in intervals of 10 seconds over a period of 180 seconds. Fluorescence intensities were normalized with unbleached ROIs of the same cells using Zeiss ZEN software. Curves of fluorescence intensity were calculated by PRISM software and half-life of fluorescence in the bleached ROIs was calculated after one-way exponential curve fitting.

CDC42 experiments

Wild-type Pac2 cells were transfected with either pEF-Bos/CDC42-V12 (Sun et al., 2000) for expression of a constitutively active CDC42 protein, or pEF-BOS/CDC42N17 (Rabiet et al., 2002) for expression of a constitutively inactive CDC42 protein. As a control, pEF-BOS backbone vector was transfected. Confluent monolayers were scratched and 5 hours later the cells were fixed and stained for Nav3a and Abi-1 by immunofluorescence.

Detection of proliferation and cell death

Proliferation in the liver bud was detected by BrdU pulse labeling analysis in *nav3a* ATG morpholino- and control morpholino-injected *Tg(sox17:GFP)*^{s870} embryos. Four hours before the indicated time points (at 22, 31, 36 and 51 hpf) BrdU was injected into the yolk sac and labeling was performed as described previously (Shin et al., 2008). At all time points the BrdU-positive cells between the pancreatic bud and the beginning pharyngeal endoderm were counted. We chose this method because *nav3a* morphant embryos lack a liver bud and this is the area from where putative hepatoblast arise. In all conditions we calculated a ratio of BrdU$^+$ cells to sox17$^+$ endodermal cells within each area.

Apoptosis in *nav3a*-ATG- and control-morpholino-injected embryos was analyzed at the indicated time points, and TUNEL staining was performed according to the manufacturer's instructions (Cell death detection kit, 12156792910, Roche).

Table 1. Real-time PCR primers

Name	Sequence (5′-3′)	Species
zf Nav3a (forward)	ATCCAGATAATAGCTAATGAGAA	zebrafish
zf Nav3a (reverse)	CAGGATGAAGAACAGACCCAG	
zf EF1 (forward)	GTGCTGTGCTGATTGTTGCT	zebrafish
zf EF1 (reverse)	TGTATGGGCTGACTTCCTTG	
hu NAV3a (forward)	GCTGCATCACAATTTCAGGTGGGT	human
hu NAV3a (reverse)	TTGAGATGATGCCACGTCTTCGGA	
18s (forward)	GTAACCCGTTGAACCCCATT	human
18s (reverse)	CCATCCAATCGGTAGTAGCG	

Nav3a-sox17:eGFP double staining

To analyze tissue specific *nav3a* expression between 22 and 26 hpf we analyzed co-expression of *nav3a* by ISH and *sox-17:gfp* by immunofluorescence in the same individuals (anti-GFP antibody, AB5450, Abcam; 1:200). We took color images of *nav3a* expression and *sox17:gfp*-positive endoderm in the same embryo and location. For merged pictures we transformed *nav3a* ISH color pictures to black and white, then merged them with the GFP image.

Nav3a co-immunoprecipitation

Co-immunoprecipitation was carried out with ZFL cells that were transfected with pDestTol2-CMV-Nav3a-eGFP expression vector. Three days after transfection, 500 μg of protein in the lysates was purified using an anti-Nav3 antibody (Eurogentec, Liege, Belgium). The immune complexes were separated by SDS-PAGE, transferred to a nitrocellulose membrane and detected using polyclonal rabbit anti-Nav3a antibody and anti f-actin antibody (Sigma, A1978).

Statistics

Comparison of numerical data was performed using Student's *t*-test. $P<0.05$ was considered to be statistically significant. Data are presented as mean ± s.e.m.

RESULTS

Zebrafish *nav3a* is an ortholog of *unc-53* and is expressed in the intestinal endoderm and the developing liver bud

We identified two *nav3* isoforms, *nav3a* and *nav3b*, that are expressed during zebrafish endoderm development (Fig. 1; see Fig. S1 in the supplementary material). By northern blot and RACE, we confirmed the existence of two *nav3* isoforms (see Fig. S1A,B in the supplementary material) and by using the respective sequence information we cloned and sequenced the longer isoform *nav3a* (Fig. 1A; see Fig. S2 in the supplementary material). Similar to *Nav3* isoforms in mouse, rat and human and to *unc-53* in *C. elegans*, zebrafish *nav3a* contains a putative calponin-like domain in its N-terminal region, which has been shown to be essential for interaction with actin filaments (Schmidt et al., 2009) (Fig. 1A; see Fig. S1C in the supplementary material). Phylogenetic alignment revealed that zebrafish Nav3a protein is closely related to *Takifugu* and *Tetraodon* Nav3 sequences (Fig. 1B).

Endodermal *nav3a* expression was found to be temporally and spatially restricted to the earliest liver specification events during zebrafish development (Fig. 1C, boxed area). *Nav3a* mRNA expression was initiated in the gut endoderm 22 hours post fertilization (hpf) in an area known to be the origin of hepatic precursor cells (Fig. 1C). Endodermal *nav3a* expression was established earlier than common markers of the budding liver including *hhex* and *prox1* (Fig. 1D). At 40 hpf, *nav3a* expression expanded to the newly formed liver bud (Fig. 1C) and was immediately downregulated after termination of primary liver formation (see Fig. S1D in the supplementary material). Between 22 hpf and 26 hpf, the *nav3a* expression domain changed rapidly

in association with morphological changes occurring within the foregut endoderm (see Fig. S1E,F in the supplementary material). During that period the foregut endoderm was getting more compact (see Fig. S1E in the supplementary material) and *nav3a* was co-expressed with the endodermal marker *sox17* (see Fig. S1F in the supplementary material).

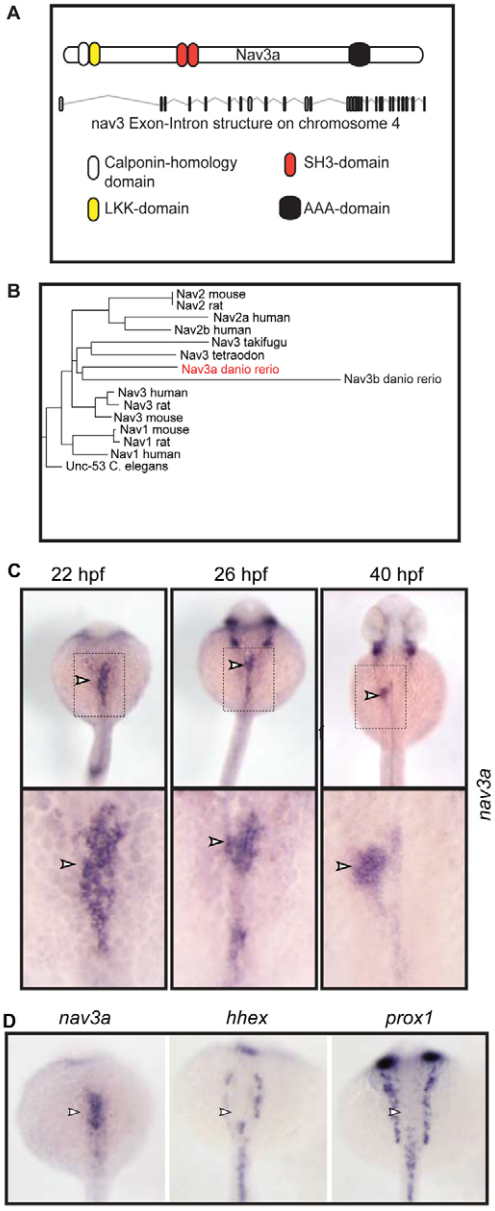

Fig. 1. Nav3a is expressed during liver development. (**A**) Nav3a contains a calponin-homology domain, an LKK-actin binding domain, a putative SH3 domain and ATPase domains of the AAA type. (**B**) Nav3a is highly related to Nav3 members of other species. (**C**) Whole-mount in situ hybridization for *nav3a* in zebrafish embryos. The boxed areas in the upper panels are presented at higher magnification in the lower panels. At 22 hpf, *nav3a* expression could be detected predominantly in the intestinal endoderm (arrowhead, left panel). Between 26 and 40 hpf, endodermal *nav3a* expression expands to the newly formed liver bud (arrowhead, middle and right panel). (**D**) Expression of *nav3a* and the early liver markers *hhex* and *prox1* analyzed by in situ hybridization in zebrafish embryos at 22 hpf. *Nav3a* expression could be detected in the foregut endoderm (arrowhead, left panel). *hhex* and *prox1* expression is limited to pancreatic precursors but is not detectable in the presumptive liver bud region (arrowhead, middle and right panel). C and D show dorsal views.

Nav3a affects liver budding and liver growth

In zebrafish embryos, knockdown of *nav3a* by injection of an ATG targeting antisense morpholino resulted in depletion of Nav3a protein expression and a blockade of liver bud formation in vivo (Fig. 2A,B; see Fig. S3A-D in the supplementary material). Compared with control embryos, a reduced outgrowth of hepatoblasts from the intestinal endoderm could be observed (Fig. 2A,B). Similar results were obtained with the splicing blocking morpholino (see Fig. S3E in the supplementary material). Developmental stage-dependent pigmentation and body shape were comparable in control and *nav3a* morpholino-injected embryos (see Fig. S3B,C in the supplementary material) but expression of the hepatocyte marker *ceruloplasmin* (*cp*) (Korzh et al., 2001) was reduced in *nav3a* morphants (see Fig. S4A in the supplementary material). Induction of exogenous endodermal *nav3a* expression under control of the *sox17* promoter, rescued liver budding defects in a major subset of *nav3a* morphants (Fig. 2C, panel 3). Moreover, endodermal overexpression of *nav3a* induced ectopic endodermal budding (Fig. 2C, right panel) and in some of the analyzed embryos we also noted dislocated endodermal cells (Fig. 2C, right panel). Interestingly, ectopic endodermal-derived buds outside the foregut region consisted predominantly of cells that expressed the early liver and pancreatic marker *hhex* (see Fig. S4B in the supplementary material), and the hepatocyte differentiation marker *ceruloplasmin* (see Fig. S4C in the supplementary material), indicating liver-like properties. To determine the long term effects of *nav3a* depletion on liver development, we analyzed liver size of late-stage *nav3a* morphant embryos and found that the liver remained strikingly reduced compared with control morpholino-injected embryos (Fig. 2B; see Fig. S3E in the supplementary material). To confirm smaller liver size on the molecular level, we analyzed expression of *c-met* (*met* – Zebrafish Information Network) as a marker for the growing liver, and detected a significantly reduced hepatic *c-met* expression domain in *nav3a*-depleted embryos (see Fig. S13 in the supplementary material). These data indicate that *nav3a* depletion induced a robust and lasting disturbance of liver development by influencing the initial budding of hepatoblasts and that aberrant liver budding in *nav3a* morphants was not compensated for at later stages.

As the temporal and spatial expression pattern of *nav3a* correlated with the earliest liver specification events, and loss of *nav3a* resulted in disturbed liver budding, *nav3a* might affect the initial steps of liver organogenesis. In zebrafish this phase is characterized by hepatoblast determination in the intestinal endoderm, followed by lateral movement of hepatic precursors (Field et al., 2003; Ober et al., 2003). We analyzed *hhex*, *foxA1* and Prox1, molecular markers of early hepatic cell fate (Ho et al., 1999; Ober et al., 2006; Odenthal and Nusslein-Volhard, 1998) and found that *nav3a* influenced hepatic outgrowth without inhibiting expression of these early hepatoblast markers (Fig. 2D,E). Before onset of liver budding, expression of *hhex* and *foxA1* was not lost in *nav3a*-depleted embryos. Instead, *nav3a* depletion predominantly affected the anatomical localization of early liver marker expression domains. *hhex*- and *foxA1*-positive hepatoblasts remained localized around the midline. Prox1 marks the earliest liver specification events (Sosa-Pineda et al., 2000) and was found to be independent of *nav3a* during the hepatoblast determination phase (Fig. 2D). We examined apoptosis and proliferation in the

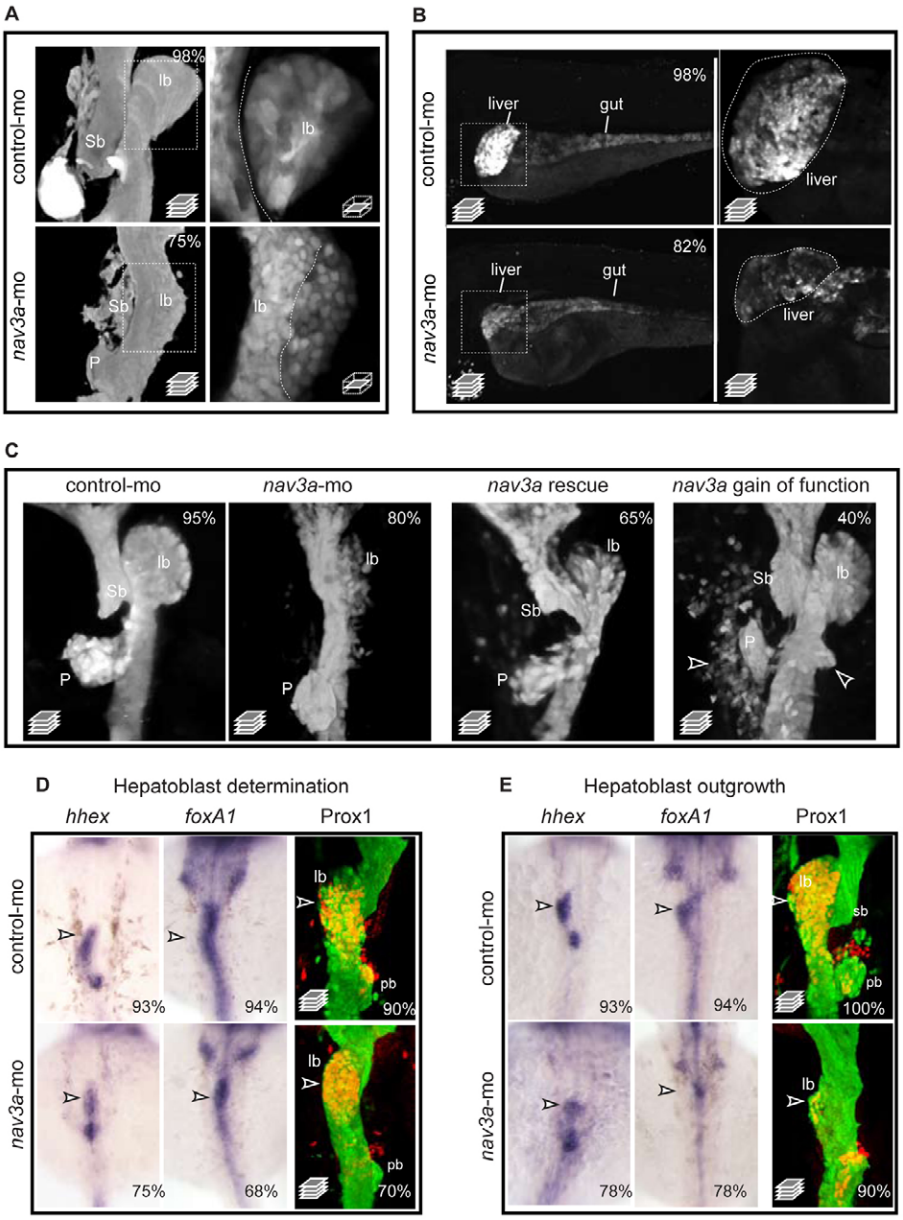

Fig. 2. Nav3a depletion reduces liver budding and growth. (**A**) Representative confocal stack pictures of *sox17:gfp* embryos shows reduced liver budding in *nav3a* morphant embryos (lower-left panel) compared with normal liver budding in control morpholino-injected embryos (upper-left panel). In *nav3a* morphants, hepatoblasts did not separate from intestinal epithelium (lower-right panel) as observed in control embryos (upper-right panel, separation line indicated). Boxed areas in left-hand panels are shown at higher magnification at a single plane in right-hand panels. (**B**) Representative confocal stack pictures of *sox17:gfp* embryos shows reduced liver growth in *nav3a* morphant embryos (lower-left panel) compared with normal liver organogenesis in control morpholino-injected embryos (upper-left panel). Higher magnifications (right) of boxed areas confirmed smaller and irregular shaped livers in *nav3a* morphant embryos (lower-right panel) compared with control embryos (upper-right panel). (**C**) Exogenously endodermal *nav3a* overexpression normalized liver budding defects in *nav3a* morpholino-injected embryos (third panel) and *nav3a* overexpression resulted in ectopic budding and dislocated endodermal cells (fourth panel). Arrowheads indicate ectopic endodermal buds or cells. In the Nav3a rescue experiment, a *nav3a* isoform mutated for the *nav3a*-ATG morpholino binding site driven by the endodermal specific promoter *sox17* was used. Images in A, C are at 40 hpf. Images in B are at 5 days pf. (**D**) Zebrafish embryos injected with control morpholino (upper panels) or *nav3a*-ATG morpholino (lower panels) were examined for expression of *hhex* (26 hpf) and *foxA1* (26 hpf) by in situ hybridization and for activated Prox1 by immunofluorescence staining (33 hpf). Before onset of liver budding, *hhex* and *foxA1* expression was only slightly reduced in *nav3a* morphants. Remaining *hhex* and *foxA1* expression could be detected at the midline (lower panels, arrowheads). Hepatic Prox1 protein activation was not significantly reduced in *nav3a* morphants (lower-right panel, arrowhead). (**E**) Analysis of the hepatoblast outgrowth phase at 40 hpf. In *nav3a* morphants (lower panels, arrowheads), *hhex* and *foxA1* expression domains differed from control embryos (upper panels, arrowheads), and Prox1 was greatly reduced. In *nav3a* morphants, some *hhex* and *foxA1* expression remained compatible with the presence of a hepatoblast population that failed to migrate laterally. lb, liver bud; sb, swim bladder primordium; P, pancreas; pb, pancreatic bud. The percentage of embryos exhibiting a phenotype as shown is indicated in the right-hand corners. *n*=150 per group in A,B; *n*=50 per group in C; *n*=8-20 per group in D. A and C show ventral view; B shows lateral view; D and E show dorsal view.

liver bud region but failed to detect significant differences between *nav3a* morphants and controls (see Fig. S5 in the supplementary material). In addition, we counted the number of *sox17-gfp* and Prox1 double-positive cells in this region (see Fig. S10 in the supplementary material). We observed no significant differences in the number of *sox-17*-Prox1 double-positive cells between *nav3a* morphants and controls during early stages (see Fig. S10 in the supplementary material). These findings suggest that it is not likely that changes in apoptosis or proliferation, or a reduction in the number of specified hepatoblasts account for the reduced liver size. By contrast, during the liver budding phase at 40 hpf, Prox1 protein expression and the number of *sox17*-Prox1 double-positive cells was significantly reduced after *nav3a* depletion (Fig. 2E; see Fig. S10 in the supplementary material). Moreover, at this time also, *hhex* and *foxA1* expression domains were greatly reduced (Fig. 2E). These data suggest that depletion of *nav3a* resulted in a failure of hepatoblasts to move out from the endoderm and that loss of migratory behavior in hepatoblasts might affect maintenance of their liver cell fate. Taken together, these data support the hypothesis that well-balanced *nav3a* expression is essential for coordinated outgrowth of hepatoblasts without affecting their initial specification.

Interestingly, comparable *nav3a*-dependent effects could also be observed in pancreatic and swim bladder morphogenesis. *nav3a* depletion negatively affected budding of the dorsal pancreas without affecting specification events (Fig. 2A; see Fig. S3F in the supplementary material). At 26 hpf, before onset of dorsal pancreatic budding, the expression of the pancreatic marker *islet-1* (*isl1* – Zebrafish Information Network) was comparable in *nav3a* morphants and controls, suggesting that dorsal pancreas specification occurred independently of *nav3a* (see Fig. S3F in the supplementary material). Also, during dorsal pancreatic budding stages *islet-1* expression appeared to be unaffected in *nav3a* morphants (see Fig. S3F in the supplementary material, right panel). In 48% of *nav3a* morphants we observed no dorsal pancreatic budding at this stage (see Fig. S3F in the supplementary material, bottom middle panel); and in a small subset of *nav3a* morphants (24%) we observed some dorsal pancreatic budding events. However, in both settings, endodermal *islet-1* expression was detectable at the position where the dorsal pancreas normally forms (see Fig. S3F in the supplementary material, bottom middle and right panel). Also, the morphogenesis of the ventral pancreas is affected in *nav3a* morphants (see Fig. S12A,B and Movies 5, 6 in the supplementary material). We analyzed Prox1 expression as a marker for ventral pancreas development at 40 hpf and found that in *nav3a* morphants Prox1 is reduced strikingly (see Fig. S12B in the supplementary material). We thus conclude that *nav3a* seems to be relevant for the morphogenesis of both liver and pancreas. We next focused on liver development in more detail.

To analyze *nav3a* function during the initial stages of hepatoblast migration, we performed in vivo time-lapse microscopy of liver budding. We imaged liver development in *sox17:gfp* transgenic zebrafish embryos between 26 hpf and 54 hpf by time-lapse confocal microscopy and demonstrated that *nav3a* is essential for hepatoblast outgrowth in vivo (Fig. 3A). The first morphological change during onset of liver formation was a thickening of the endodermal rod, cranial to the already established pancreatic bud. Subsequently, a population of putative hepatoblast precursors separated from the intestinal endoderm and migrated away from the endoderm to form a defined liver bud (Fig. 3A; see Movie 1 and Fig. S11 in the supplementary material). By contrast, in *nav3a* morphant embryos the hepatoblasts remained connected to the intestinal endoderm, suggesting that *nav3a* is essential for outward movement of hepatoblasts (Fig. 3A, lower panels; see Movie 2 in the supplementary material). Migration out of the endoderm was not detected over a time period of up to 15 hours (Fig. 3A; see Movie 2 in the supplementary material). As we could not detect differences in hepatoblast proliferation or apoptosis (see Fig. S5 in the supplementary material), these data argue for a specific role of *nav3a* in the migration of hepatoblasts in vivo. In line with these observations, *nav3a* knockdown in zebrafish and human cell lines

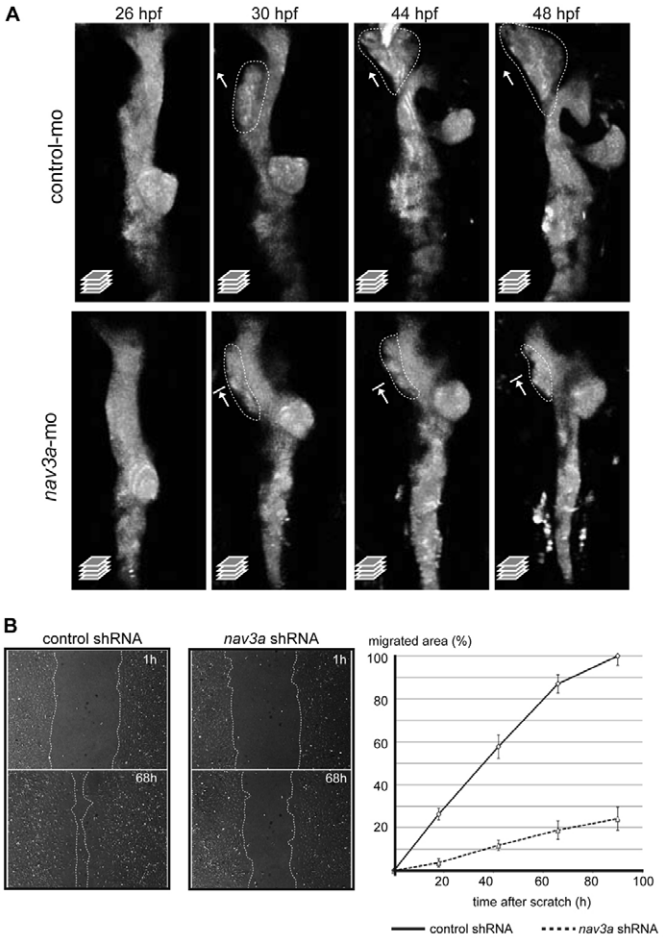

Fig. 3. Nav3a controls hepatoblast movement from the intestinal endoderm. (**A**) Confocal time-lapse imaging of liver development in *sox17:gfp* embryos 26-48 hpf after injection of control morpholino (upper panels) or *nav3a*-ATG morpholino (lower panels). In control embryos, the endodermal rod thickened (upper panel, 26 hpf). Subsequently, a cell population on the left side, cranial to the pancreatic bud separated from the intestinal endoderm (upper panel, 30 hpf) and migrated in a leftward direction to form the liver bud (upper panels, 30-48 hpf). *Nav3a* depletion reduced outgrowth of hepatoblasts resulting in a smaller liver bud (lower panels, 30-48 hpf). All images show a dorsal view; dotted lines demarcate putative hepatoblast populations and arrows depict outgrowth direction. (**B**) Pac-2 zebrafish cells stably expressing control shRNA or *nav3a* shRNA were analyzed in an in vitro scratch-migration assay. Confluent monolayers were scratched and at the indicated time points the migrated area was measured in control (B, left panels) and *nav3a* knockdown cells (B, middle panels). *Nav3a* depletion significantly reduced the migratory capacity (B, right panel; $P<0,001$; mean ± s.e.m.); $n=6$-12 scratched areas from three separate experiments.

strikingly reduced directed migration in two different (hepatic) cell lines in vitro. In *nav3a* depleted zebrafish cells, migration capacity was reduced profoundly (Fig. 3B; see Movie 3 and Fig. S6A in the supplementary material). In addition, *NAV3a* siRNA-treated human liver cells also migrated significantly slower than respective control cells (see Fig. S6B in the supplementary material).

To characterize the molecular mechanism by which *nav3a* controls migration at the cellular level, we analyzed its intracellular localization by immunostaining (see Fig. S9 in the supplementary material for verification of antibody staining). Thus far, endogenous subcellular and tissue specific expression of the *Nav3a* isoform in vertebrates have not been shown. In quiescent cells, we found that Nav3a protein was localized exclusively in the Golgi apparatus. However, in migrating hepatic cells, Nav3a protein associated with lamellipodia and filipodia both in vitro (Fig. 4A,B; see Fig. S7D in the supplementary material) and in vivo (see Fig. S7A,B in the supplementary material), suggesting that during migratory events the protein was shuttled to cellular protrusions.

UNC-53, the nematode Nav3a homolog, interacts with ABI-1, a molecule known to associate with the ARP2/3 complex. Because the calponin-like homology domain of UNC-53 mediates the interaction with ABI-1 (Schmidt et al., 2009) and Nav3a also shares this domain, we tested whether Nav3a associates with Abi1 in zebrafish cells. Immunofluorescence analysis demonstrated colocalization of Nav3a, Abi1 and actin filaments in protrusions of migrating cells (Fig. 4B). Furthermore, actin polymerization in these cell protrusions was significantly reduced after knockdown of *nav3a* (Fig. 4C,D). To confirm that zebrafish Nav3a protein interacts with actin, we overexpressed a Nav3a-GFP fusion protein in hepatocytes, and performed a co-immunoprecipitation of f-actin with anti-Nav3a (see Fig. S7C in the supplementary material). The Western blot of Nav3a-precipitated protein lysate revealed co-immunoprecipitation of f-actin and Nav3a, thus confirming that Nav3a interacts physically with actin (see Fig. S7C in the supplementary material). Moreover, we could detect Nav3a-actin interaction at actin branching points in filopodia protrusion of motile zebrafish liver cells, thus supporting a role for Nav3a in actin filament remodeling (see Fig. S7D and Movie 4 in the supplementary material).

GTPases, including Cdc42, are major players in mediating lamellipodia and filipodia formation during cell migration. We tested whether Cdc42 activity influences Nav3a localization during cell migration (Bompard and Caron, 2004; Takenawa and Suetsugu, 2007; Heasman and Ridley, 2008; Rohatgi et al., 1999; Stradal et al., 2004; Takenawa and Suetsugu, 2007). Indeed activation of Cdc42 resulted in the emergence of Nav3a protein in cell protrusions of migrating cells (Fig. 4E-G). Taken together, these data suggest a dynamic role of Nav3a in modulating actin polymerization during hepatoblast outgrowth in the context of liver organogenesis.

Data generated from mouse and zebrafish indicate that hepatic organogenesis is induced in response to members of the Wnt family, fibroblast growth factors (FGFs) and bone morphogenetic proteins (BMPs) (Calmont et al., 2006; Jung et al., 1999; Ober et al., 2006; Rossi et al., 2001; Shin et al., 2007; Zaret, 2002). Wnt2bb is described as one of the earliest inductive sources of liver specification in zebrafish (Ober et al., 2006). Also BMP-receptor-1 and FGF-receptor-1 are essential mediators of liver specification in zebrafish embryogenesis (Lee et al., 2005; Pyati et al., 2005; Shin et al., 2007). It has previously been shown that heat shock inducible expression of dominant-negative BMP-receptor-1 and dominant-negative FGF-receptor-1 leads to an effective block of all relevant BMP and FGF family members (Lee et al., 2005; Pyati et al., 2005; Shin et al., 2007). We utilized heat shock-inducible expression of dominant-negative BMP-receptor-1, a dominant-negative FGF-receptor-1 and morpholino-mediated depletion of *wnt2bb* to block respective signaling pathways in zebrafish embryogenesis and to analyze their impact on *nav3a* expression. We found expression of *nav3a* and the hepatic marker *hhex* to be reduced in *wnt2bb* morphant embryos (Fig. 5A; see Fig. S8 in the supplementary material). After inhibition of FGF- and BMP-receptor signaling, *hhex* expression in the liver bud was reduced significantly (see Fig. S8 in the supplementary material) (Shin et al., 2007). However, *nav3a* expression was not affected in both dominant-negative BMP-receptor-1 and dominant-negative FGF-receptor-1 transgenic zebrafish embryos (Fig. 5B,C). These data suggest that initiation of *nav3a* transcription during embryogenesis involves a *wnt2bb* signaling component, but is independent of BMP- and FGF-receptor 1 signaling. In line with this, inhibition of *wnt2bb* phenocopied aberrant liver budding, as observed in *nav3a* depleted embryos (Fig. 5D). Additionally, overexpression of *nav3a* in *wnt2bb* morphants resulted in re-emergence of liver budding events in a subset of *wnt2bb* morphants (Fig. 5E). Although liver morphogenesis was not completely restored in this rescue approach, and *wnt2bb* might exert effects on other factors beyond *nav3a*, these data argue for *wnt2bb*-dependent control of *nav3a* synthesis in vivo.

DISCUSSION

Our study was initiated by the concept that neural guidance genes might exert a functional role in tissue morphogenesis beyond the nervous system. Neural guidance gene function has been well documented in the nematode. Genetic screens of nematode locomotor mutants (*uncoordinated*, *unc*) led to the discovery of several ligands and receptors relevant for commissural and motor axon guidance, including UNC-5 and the ligand UNC-6 (a netrin) (Leung-Hagesteijn et al., 1992; Chan et al., 1996; Ishii et al., 1992). Studies in higher vertebrates subsequently showed that their function in the developing nervous system is preserved (Leonardo et al., 1997; Serafini et al., 1996), and even extends to the growing vascular system (Lu et al., 2004). This led to the concept that during evolution neural guidance gene function has been co-opted by the developing vascular system to mediate guidance events (Lu et al., 2004). The extent to which neural guidance genes can play a functional role in shaping other organs has not been explored well. Because movement of cells to their predetermined position is relevant for establishing endodermal organogenesis, we examined whether neural guidance genes play a role herein.

In *C. elegans*, UNC-53 appears to act cell autonomously in migration and outgrowth of axons (Stringham et al., 2002). Here, we show novel findings demonstrating that a zebrafish homolog of UNC-53, Neural navigator 3a (Nav3a), is relevant for determining endodermal liver development, involving actin remodeling in lamellipodia and filipodia of migrating liver cells. *nav3a* is expressed in the early foregut endoderm in the region giving rise to the liver, and knockdown of *nav3a* in vivo results in a strikingly reduced liver size. In *nav3a* morphants, expression of the liver markers *hhex*, *foxA1* and Prox1 is not affected during early stages of liver development, suggesting that initial hepatoblast specification can occur in *nav3a* morphants. In support of this, the number of sox17-Prox1 double-positive cells was comparable in *nav3a* morphants and controls. However, expression of *hhex*, *foxA1* and Prox1 is progressively lost during the hepatoblast outgrowth

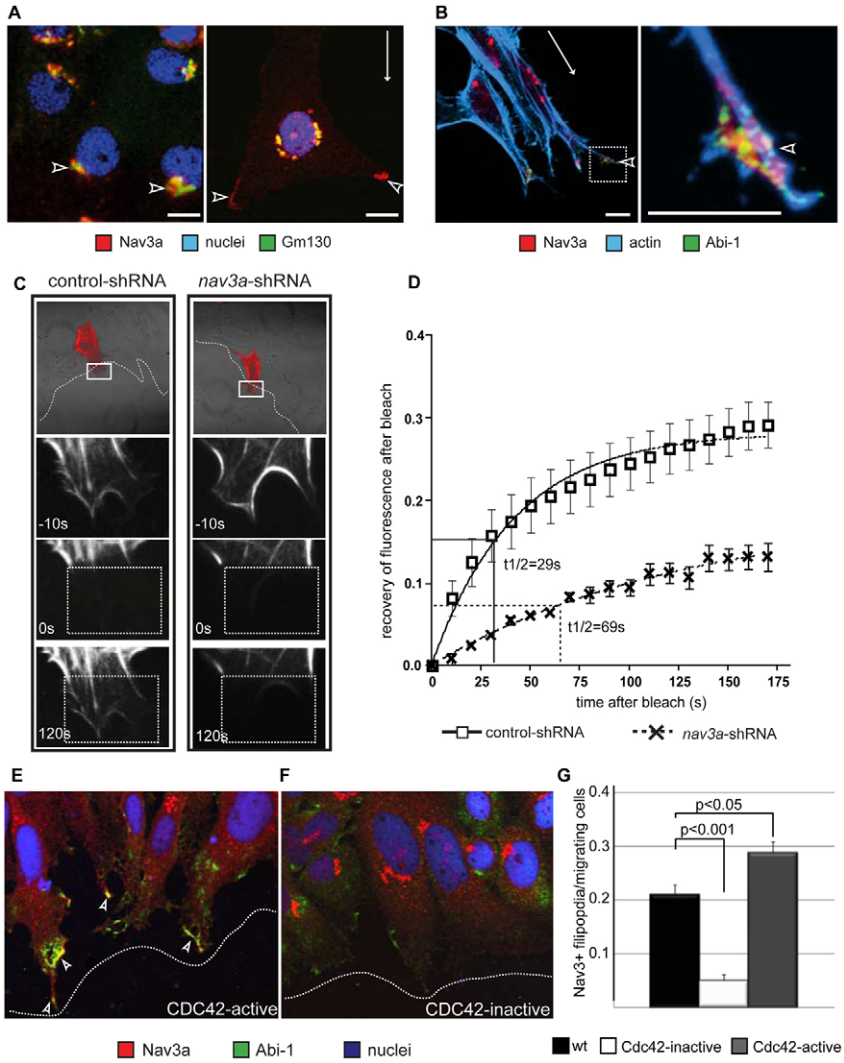

Fig. 4. Nav3a regulates actin in cell protrusions of moving cells. (**A**,**B**) Nav3a, actin and Abi1 immunofluorescence staining in quiescent and migrating ZFL liver cells. White arrows indicate the direction of migration. In non-migrating cells Nav3a localizes in the Golgi apparatus and here it colocalizes with the Golgi matrix protein gm130 (A, left-hand panel, arrowheads). In migrating cells, Nav3a is localized in distal ends of cell protrusions (A, right-hand panel, white arrowhead). Nav3a, Abi-1 and actin co-localized in distal ends of filipodia and lamellipodia (B, left-hand panel, white arrowheads) of migrating cells. Right-hand panel in B is a higher magnification of the boxed area in the left-hand panel. (**C**,**D**) *Nav3a* regulates actin polymerization dynamics in cell protrusions of migrating cells. Pac-2 cells stably expressing control shRNA or Nav3a shRNA were analyzed for actin polymerization dynamics by the FRAP (fluorescence recovery after photobleaching) assay. Cells were transfected with a vector coding the actin binding protein lifeact-RFP and scratch assays were performed. Representative pictures of fluorescence recovery after photobleaching showed that in Nav3a-deficient cells fluorescence-labeled actin bundles recovered more slowly compared with control cells (C, left-hand panels control; right-hand panels Nav3a deficient). (D) The recovery kinetics of lifeact-RFP after photobleaching, together with the half-life (t1/2) data. *n*=15 per group, data are presented as mean ± s.e.m. The FRAP experiments were repeated three times. Boxed areas in top panel are shown at higher magnification below. Dotted boxed areas indicate area of photobleaching. (**E-G**) Cdc42 mediates Nav3a protein translocation to cellular protrusions during cell migration. (E) Pac-2 cells were transfected with a constitutively active form of Cdc42. Activation of Cdc42 resulted in Nav3a translocation to distal ends of filipodia. (F) Transfection of inactive Cdc42-N17 inhibited Nav3a translocation. Arrowheads indicate Abi1-Nav3a double-positive cells. Dotted lines indicate the migration front. (G) Quantification of filipodia formation. *n*=300 cells per group, data are presented as mean ± s.e.m.

stage, concomitantly with a reduction in liver budding in *nav3a* morphants. Because proliferation or apoptosis rates in the liver bud are comparable between *nav3a* morphants and controls, we speculate that the loss of hepatocyte marker expression in *nav3a* morphants at later stages is most likely to be a consequence of the migration defect. We speculate that the cells that fail to move might subsequently integrate in the unspecified foregut endoderm. Our data show that the reduced liver size in *nav3a* morphants probably reflects a defect in hepatoblast movement out from the gut endoderm. In line with this, in vivo time-lapse imaging showed that in *nav3a* morphants the budding movement of endodermal cells from the endoderm, in the region known to give rise to the liver, was severely disturbed. This budding defect could be rescued by re-introducing *nav3a* mRNA to the endoderm, indicating that the liver phenotype in *nav3a* morphants involves a specific contribution of *nav3a*.

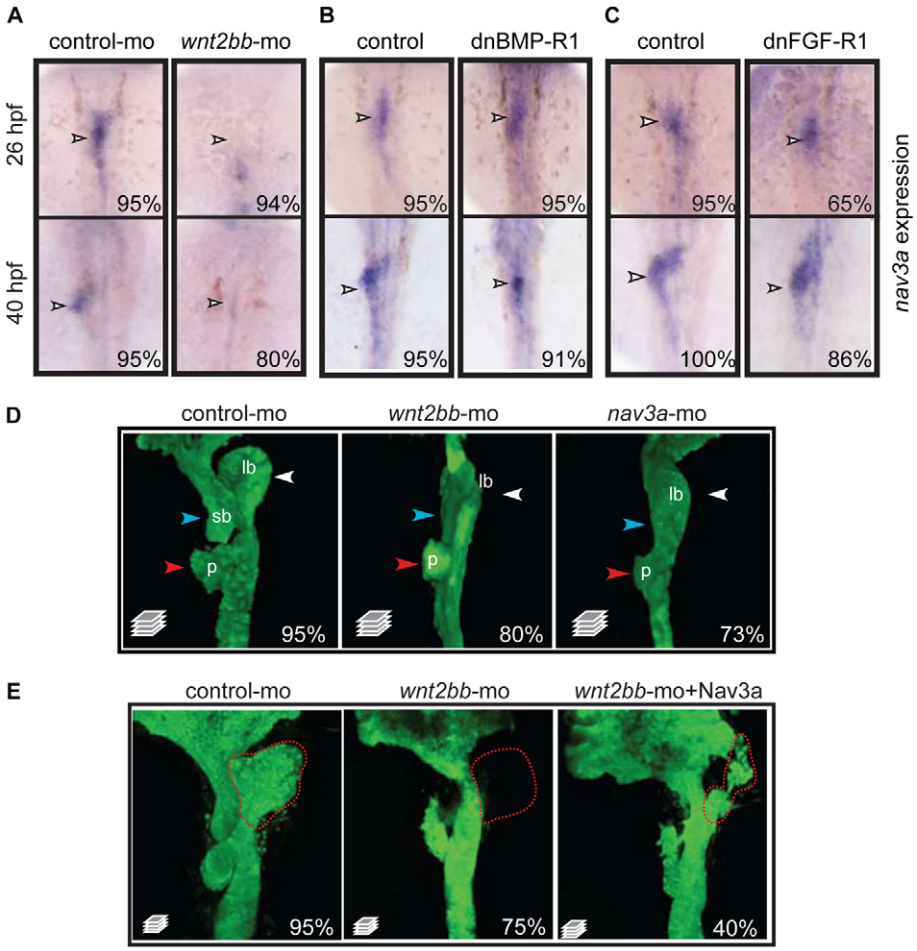

Fig. 5. Nav3a expression is controlled by Wnt2bb signaling. (**A**) Embryos injected with control morpholino or *wnt2bb* morpholino examined for *nav3a* expression by in situ hybridization. *Wnt2bb* inhibition results in reduced *nav3a* expression in the liver bud (arrowheads). (**B**,**C**) Embryos obtained from outcrossing of hemizygous *Tg*(*hsp70l:dnBmpr-GFP*) or *Tg*(*hsp70l:dnfgfr1-GFP*) zebrafish were heat shocked at 18 hpf, collected at 40 hpf and examined for *nav3a* expression by in situ hybridization. Inhibition of BMP and FGF receptor signaling did not annihilate *nav3a* expression (arrowheads) in the liver bud. (**D**) *Wnt2bb* depletion phenocopies *nav3a* depletion. *Sox17:gfp* embryos injected either with control morpholino (left-hand panel), *wnt2bb* morpholino (middle panel) or *nav3a*-ATG morpholino (right-hand panel) examined at 40 hpf by confocal microscopy. Both *wnt2bb*- and *nav3a*-morphant embryos developed an aberrant liver bud (white arrowhead). Also the pancreatic bud and the swim bladder primordium did not develop properly (red and blue arrowheads, respectively). (**E**) Endodermal *nav3a* overexpression partially rescued *wnt2bb* inhibition. *Sox17-gfp* embryos were injected with control morpholino, *wnt2bb* morpholino alone or *wnt2bb* morpholino together with *sox17-nav3a*-mcherry plasmid and analyzed at 50 hpf. *Wnt2bb* inhibition induced aberrant development of the liver bud, pancreatic bud and swim bladder primordium (middle panel). In 40% of embryos, endodermal *nav3a* overexpression results in a partial rescue of liver bud formation (right-hand panel). Nevertheless these liver buds appeared to be aberrantly shaped (right-hand panel). Red dotted lines indicate the liver bud. The percentage of embryos exhibiting a similar phenotype as displayed in the figure, is indicated in the lower right-hand corner (A-C: *n*=10-30 embryos per group; D: *n*=150 per group, E; *n*=100 per group). lb, liver bud; sb, swim bladder primordium; p, pancreatic bud. A-C show dorsal view; D and E show ventral view.

As the structure of Nav3a predicts interaction with proteins relevant for cytoskeleton remodeling, we examined this in more detail. Owing to technical limitations with respect to high resolution imaging of lamellipodia and actin remodeling events in hepatoblasts in vivo, we turned to an in vitro model system. We provide several lines of evidence showing a functional role for Nav3a in actin remodeling and cell migration. First, in quiescent cells in vitro Nav3a protein is stored in the Golgi apparatus, but in migrating cells Nav3a translocates to the filipodia and lamellipodia. Second, loss of *nav3a* reduces actin-remodeling events in cell protrusions, concomitantly with loss of migration capacity. Third, we show that in migrating cells Nav3a interacts physically with the actin-cytoskeleton in filipodia. Such interactions are especially clear at actin branching points in the spike-like actin extensions of filipodia protrusions. These data suggest that *nav3a* might act as a positive modulator of actin polymerization in lamellipodia and filipodia extensions, which is required for cell movement.

Abi1 is essential for cell movement during early embryogenesis (Disanza et al., 2004; Roffers-Agarwal et al., 2005) as it is involved in activation of Rho family GTPases and signal integration to actin polymerization. In migrating zebrafish cells, Nav3a protein colocalizes with Abi1 at the distal end of filipodia and lamellipodia protrusions, and here Nav3a-Abi1 interactions might positively regulate actin-remodeling events. Activation of the actin polymerization machinery, furthermore, involves GTPases of the Rho family including Cdc42 (Heasman and Ridley, 2008; Rohatgi

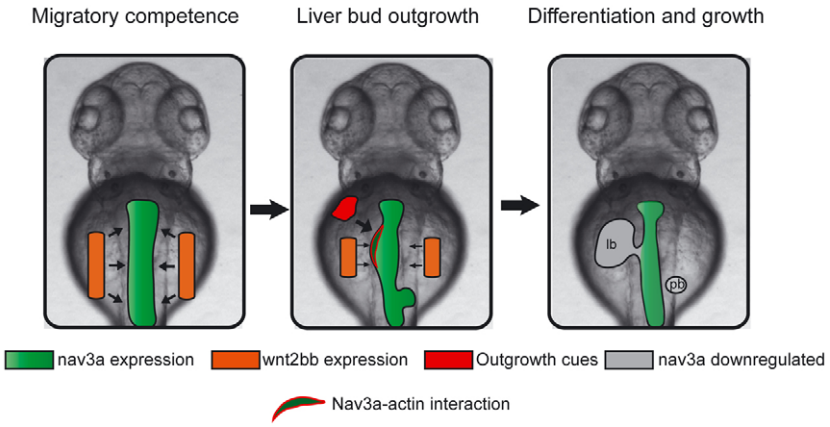

Fig. 6. The postulated model. Left: Wnt2bb initiates migratory competence in endodermal cells by controlling Nav3a synthesis in the predetermined intestinal endoderm. Middle: In a second step, FGF and BMP alone or in combination with other 'outgrowth factors' might mediate translocation of Nav3a protein from Golgi apparatus to lamellipodia and filipodia in hepatoblasts. There, Nav3a interacts with Arp2/3-Abi1-dependent actin assembly complexes. Subsequently, Nav3a positively modulates actin assembly and thereby enables migrating hepatoblasts to follow their trajectory. Right: Nav3a expression is downregulated after completion of the liver bud. lb, liver bud; pb, pancreatic bud.

et al., 1999). GTPases, such as Cdc42, control via Arp2/3 the formation of lamellipodia and filipodia (Bompard and Caron, 2004; Stradal et al., 2004; Takenawa and Suetsugu, 2007). This cascade mediates directed actin nucleation controlling assembly (Heasman and Ridley, 2008). We observe a positive correlation between Cdc42 activity and Nav3a protein localization in the cell protrusions. Annihilating Cdc42 activity impairs Nav3a translocation from the Golgi apparatus to the filipodia extensions and reduces lamellipodia and filipodia formation. Although this experiment does not prove that Cdc42 is the activator of Nav3a, it shows that, in Cdc42-activated motile cells, Nav3a protein becomes localized in the cell protrusions at the leading edge, consistent with a putative role in cellular forward movement.

It is postulated that liver specification in zebrafish is mediated by a complex interplay of Wnt2bb and members of the FGF and BMP families secreted by tissues adjacent to the intestinal endoderm (Calmont et al., 2006; Jung et al., 1999; Rossi et al., 2001; Shin et al., 2007; Zaret, 2002). Only inhibition of *wnt2bb* phenocopied the aberrant liver growth, as observed in *nav3a* morphants, and *wnt2bb* morphants show a reduction in foregut endodermal *nav3a* expression. Endodermal-specific overexpression of *nav3a* in *wnt2bb* morphants results in restoration of hepatoblast budding in a subset of embryos. Therefore, *wnt2bb* is relevant for initiating *nav3a* expression in the intestinal endoderm and we speculate that *wnt2bb*, via *nav3a*, is giving hepatoblasts the capacity to move out from the gut endoderm. As liver morphogenesis in *wnt2bb* morphants is not completely restored in our *nav3a* rescue approach, it is likely that *wnt2bb* has additional effects beyond activation of *nav3a*.

Consistent with a positive role for *nav3a* in endodermal cell movement, we show that overexpression of *nav3a* under the control of the endodermal specific promoter *sox17* in wild-type embryos results in ectopic budding along the intestinal endoderm. Ectopic budding events correlated with *nav3a* expression levels, and budding was observed up to the most posterior parts of the trunk. These observations are compatible with a model in which endodermal cells with high expression levels of *nav3a* become highly motile and migrate out from the (gut) endoderm, giving rise to ectopic buds. Interestingly, these ectopic buds express the liver markers *hhex* and *cp*, suggesting that the cells in the buds have a liver-like cell identity. One explanation for the molecular expression of liver cell markers in the ectopic buds in the gain-of-function experiments is the selective movement of specified hepatoblasts out from the foregut endoderm. However, we feel that this is rather unlikely because the ectopic buds arise at locations distant from the foregut, for example the trunk region and the yolk sac. This leaves open the possibility that during overexpression of *nav3a* in the endoderm, endodermal cells with high *nav3a* expression acquire liver marker expression. What remains to be determined is whether this is a *nav3a*-mediated cell autonomous response, or is dependent on local cues involving BMP or FGF signaling. If such BMP/FGF cues are not present throughout the embryo, it might even be speculated that movement of endodermal *nav3a*-positive cells out from the (gut) endoderm itself results in acquisition of liver markers, but such a process suggests the existence of liver cell fate repressive signaling in the gut endoderm.

Taken together, we propose a model in which during zebrafish embryogenesis *nav3a*, transcriptionally activated by *wnt2bb* signaling, provides migratory competence to hepatoblasts in the intestinal endoderm (Fig. 6). Loss of *nav3a* reduces the migratory capacity of hepatoblasts and thereby inhibits liver budding and, subsequently, hepatic organogenesis. Nav3a affects the kinetics of lamellipodia and filipodia extensions by positively modulating actin polymerization, determining cell movement. Our data furthermore support the concept that during evolution, neural guidance gene function has not only been co-opted by the vascular system, but also by developing endodermal organs to mediate tissue morphogenesis.

Acknowledgements
We thank Franz Oswald for providing lifeact-mRuby and lifeact-eosFP plasmids, Didier Stainier for providing the sox17:GFP zebrafish strain, Shiro Suetsugu for providing Cdc-42 constructs and Anje Sporbert of the MDC confocal core facility for her support. This work was funded by grants from the Helmholtz society, the Netherlands Organization for Scientific research (NWO-Vidi) and CSB (Center for Stroke research Berlin). The Zebrafish International Resource Center (ZIRC) is supported by grant P40 RR012546 from the NIH-NCRR. Deposited in PMC for release after 12 months.

Competing interests statement
The authors declare no competing financial interests.

Supplementary material
Supplementary material for this article is available at
http://dev.biologists.org/lookup/suppl/doi:10.1242/dev.056861/-/DC1

References
Bompard, G. and Caron, E. (2004). Regulation of WASP/WAVE proteins: making a long story short. *J. Cell Biol.* **166**, 957-962.
Bort, R., Signore, M., Tremblay, K., Martinez Barbera, J. P. and Zaret, K. S. (2006). Hex homeobox gene controls the transition of the endoderm to a pseudostratified, cell emergent epithelium for liver bud development. *Dev. Biol.* **290**, 44-56.
Calmont, A., Wandzioch, E., Tremblay, K. D., Minowada, G., Kaestner, K. H., Martin, G. R. and Zaret, K. S. (2006). An FGF response pathway that mediates hepatic gene induction in embryonic endoderm cells. *Dev. Cell* **11**, 339-348.
Chan, S. S., Zheng, H., Su, M. W., Wilk, R., Killeen, M. T., Hedgecock, E. M. and Culotti, J. G. (1996). UNC-40, a C. elegans homolog of DCC (Deleted in

Colorectal Cancer), is required in motile cells responding to UNC-6 netrin cues. *Cell* **87**, 187-195.
Disanza, A., Carlier, M. F., Stradal, T. E., Didry, D., Frittoli, E., Confalonieri, S., Croce, A., Wehland, J., Di Fiore, P. P. and Scita, G. (2004). Eps8 controls actin-based motility by capping the barbed ends of actin filaments. *Nat. Cell Biol.* **6**, 1180-1188.
Elias, H. (1955). Origin and early development of the liver in various vertebrates. *Acta Hepatol.* **3**, 1-57.
Era, A., Tominaga, M., Ebine, K., Awai, C., Saito, C., Ishizaki, K., Yamato, K. T., Kohchi, T., Nakano, A. and Ueda, T. (2009). Application of Lifeact reveals F-actin dynamics in Arabidopsis thaliana and the liverwort, Marchantia polymorpha. *Plant Cell Physiol.* **50**, 1041-1048.
Field, H. A., Ober, E. A., Roeser, T. and Stainier, D. Y. (2003). Formation of the digestive system in zebrafish. I. Liver morphogenesis. *Dev. Biol.* **253**, 279-290.
Goessling, W., North, T. E., Lord, A. M., Ceol, C., Lee, S., Weidinger, G., Bourque, C., Strijbosch, R., Haramis, A. P., Puder, M. et al. (2008). APC mutant zebrafish uncover a changing temporal requirement for wnt signaling in liver development. *Dev. Biol.* **320**, 161-174.
Heasman, S. J. and Ridley, A. J. (2008). Mammalian Rho GTPases: new insights into their functions from in vivo studies. *Nat. Rev. Mol. Cell Biol.* **9**, 690-701.
Ho, C. Y., Houart, C., Wilson, S. W. and Stainier, D. Y. (1999). A role for the extraembryonic yolk syncytial layer in patterning the zebrafish embryo suggested by properties of the hex gene. *Curr. Biol.* **9**, 1131-1134.
Huber, A. B., Kolodkin, A. L., Ginty, D. D. and Cloutier, J. F. (2003). Signaling at the growth cone: ligand-receptor complexes and the control of axon growth and guidance. *Annu. Rev. Neurosci.* **26**, 509-563.
Ishii, N., Wadsworth, W. G., Stern, B. D., Culotti, J. G. and Hedgecock, E. M. (1992). UNC-6, a laminin-related protein, guides cell and pioneer axon migrations in C. elegans. *Neuron* **9**, 873-881.
Jung, J., Zheng, M., Goldfarb, M. and Zaret, K. S. (1999). Initiation of mammalian liver development from endoderm by fibroblast growth factors. *Science* **284**, 1998-2003.
Klein, C., Wustefeld, T., Assmus, U., Roskams, T., Rose-John, S., Muller, M., Manns, M. P., Ernst, M. and Trautwein, C. (2005). The IL-6-gp130-STAT3 pathway in hepatocytes triggers liver protection in T cell-mediated liver injury. *J. Clin. Invest.* **115**, 860-869.
Korzh, S., Emelyanov, A. and Korzh, V. (2001). Developmental analysis of ceruloplasmin gene and liver formation in zebrafish. *Mech. Dev.* **103**, 137-139.
Lee, Y., Grill, S., Sanchez, A., Murphy-Ryan, M. and Poss, K. D. (2005). Fgf signaling instructs position-dependent growth rate during zebrafish fin regeneration. *Development* **132**, 5173-5183.
Leonardo, E. D., Hinck, L., Masu, M., Keino-Masu, K., Fazeli, A., Stoeckli, E. T., Ackerman, S. L., Weinberg, R. A. and Tessier-Lavigne, M. (1997). Guidance of developing axons by netrin-1 and its receptors. *Cold Spring Harb. Symp. Quant. Biol.* **62**, 467-478.
Leung-Hagesteijn, C., Spence, A. M., Stern, B. D., Zhou, Y., Su, M. W., Hedgecock, E. M. and Culotti, J. G. (1992). UNC-5, a transmembrane protein with immunoglobulin and thrombospondin type 1 domains, guides cell and pioneer axon migrations in C. elegans. *Cell* **71**, 289-299.
Lu, X., Le Noble, F., Yuan, L., Jiang, Q., De Lafarge, B., Sugiyama, D., Breant, C., Claes, F., De Smet, F., Thomas, J. L. et al. (2004). The netrin receptor UNC5B mediates guidance events controlling morphogenesis of the vascular system. *Nature* **432**, 179-186.
Maes, T., Barcelo, A. and Buesa, C. (2002). Neuron navigator: a human gene family with homology to unc-53, a cell guidance gene from Caenorhabditis elegans. *Genomics* **80**, 21-30.
Margagliotti, S., Clotman, F., Pierreux, C. E., Beaudry, J. B., Jacquemin, P., Rousseau, G. G. and Lemaigre, F. P. (2007). The Onecut transcription factors HNF-6/OC-1 and OC-2 regulate early liver expansion by controlling hepatoblast migration. *Dev. Biol.* **311**, 579-589.
Ober, E. A., Field, H. A. and Stainier, D. Y. (2003). From endoderm formation to liver and pancreas development in zebrafish. *Mech. Dev.* **120**, 5-18.
Ober, E. A., Verkade, H., Field, H. A. and Stainier, D. Y. (2006). Mesodermal Wnt2b signalling positively regulates liver specification. *Nature* **442**, 688-691.
Odenthal, J. and Nusslein-Volhard, C. (1998). fork head domain genes in zebrafish. *Dev. Genes Evol.* **208**, 245-258.
Peeters, P. J., Baker, A., Goris, I., Daneels, G., Verhasselt, P., Luyten, W. H., Geysen, J. J., Kass, S. U. and Moechars, D. W. (2004). Sensory deficits in mice hypomorphic for a mammalian homologue of unc-53. *Brain Res. Dev. Brain Res.* **150**, 89-101.
Pyati, U. J., Webb, A. E. and Kimelman, D. (2005). Transgenic zebrafish reveal stage-specific roles for Bmp signaling in ventral and posterior mesoderm development. *Development* **132**, 2333-2343.
Rabiet, M. J., Tardif, M., Braun, L. and Boulay, F. (2002). Inhibitory effects of a dominant-interfering form of the Rho-GTPase Cdc42 in the chemoattractant-elicited signaling pathways leading to NADPH oxidase activation in differentiated HL-60 cells. *Blood* **100**, 1835-1844.
Reim, G., Mizoguchi, T., Stainier, D. Y., Kikuchi, Y. and Brand, M. (2004). The POU domain protein spg (pou2/Oct4) is essential for endoderm formation in cooperation with the HMG domain protein casanova. *Dev. Cell* **6**, 91-101.
Roffers-Agarwal, J., Xanthos, J. B. and Miller, J. R. (2005). Regulation of actin cytoskeleton architecture by Eps8 and Abi1. *BMC Cell Biol.* **6**, 36.
Rohatgi, R., Ma, L., Miki, H., Lopez, M., Kirchhausen, T., Takenawa, T. and Kirschner, M. W. (1999). The interaction between N-WASP and the Arp2/3 complex links Cdc42-dependent signals to actin assembly. *Cell* **97**, 221-231.
Rossi, J. M., Dunn, N. R., Hogan, B. L. and Zaret, K. S. (2001). Distinct mesodermal signals, including BMPs from the septum transversum mesenchyme, are required in combination for hepatogenesis from the endoderm. *Genes Dev.* **15**, 1998-2009.
Schmidt, K. L., Marcus-Gueret, N., Adeleye, A., Webber, J., Baillie, D. and Stringham, E. G. (2009). The cell migration molecule UNC-53/NAV2 is linked to the ARP2/3 complex by ABI-1. *Development* **136**, 563-574.
Serafini, T., Colamarino, S. A., Leonardo, E. D., Wang, H., Beddington, R., Skarnes, W. C. and Tessier-Lavigne, M. (1996). Netrin-1 is required for commissural axon guidance in the developing vertebrate nervous system. *Cell* **87**, 1001-1014.
Shin, C. H., Chung, W. S., Hong, S. K., Ober, E. A., Verkade, H., Field, H. A., Huisken, J. and Stainier, D. Y. (2008). Multiple roles for Med12 in vertebrate endoderm development. *Dev. Biol.* **317**, 467-479.
Shin, D., Shin, C. H., Tucker, J., Ober, E. A., Rentzsch, F., Poss, K. D., Hammerschmidt, M., Mullins, M. C. and Stainier, D. Y. (2007). Bmp and Fgf signaling are essential for liver specification in zebrafish. *Development* **134**, 2041-2050.
Si-Tayeb, K., Lemaigre, F. P. and Duncan, S. A. (2010). Organogenesis and development of the Liver. *Dev. Cell* **18**, 175-189.
Sosa-Pineda, B., Wigle, J. T. and Oliver, G. (2000). Hepatocyte migration during liver development requires Prox1. *Nat. Genet.* **25**, 254-255.
Stradal, T. E., Rottner, K., Disanza, A., Confalonieri, S., Innocenti, M. and Scita, G. (2004). Regulation of actin dynamics by WASP and WAVE family proteins. *Trends Cell Biol.* **14**, 303-311.
Stringham, E., Pujol, N., Vandekerckhove, J. and Bogaert, T. (2002). unc-53 controls longitudinal migration in C. elegans. *Development* **129**, 3367-3379.
Sun, H., King, A. J., Diaz, H. B. and Marshall, M. S. (2000). Regulation of the protein kinase Raf-1 by oncogenic Ras through phosphatidylinositol 3-kinase, Cdc42/Rac and Pak. *Curr. Biol.* **10**, 281-284.
Takenawa, T. and Suetsugu, S. (2007). The WASP-WAVE protein network: connecting the membrane to the cytoskeleton. *Nat. Rev. Mol. Cell Biol.* **8**, 37-48.
Tran, T. S., Kolodkin, A. L. and Bharadwaj, R. (2007). Semaphorin regulation of cellular morphology. *Annu. Rev. Cell Dev. Biol.* **23**, 263-292.
Vidali, L., Rounds, C. M., Hepler, P. K. and Bezanilla, M. (2009). Lifeact-mEGFP reveals a dynamic apical F-actin network in tip growing plant cells. *PLoS One* **4**, e5744.
Westerfield, M. (2000). *The Zebrafish Book. A Guide for the Laboratory use of Zebrafish (*Danio rerio*)*. Eugene, OR: University of Oregon Press.
Zaret, K. S. (2002). Regulatory phases of early liver development: paradigms of organogenesis. *Nat. Rev. Genet.* **3**, 499-512.